

CHAPTER IV
DIRECTING THERMOPLASTIC ELASTOMER MICRODOMAIN
PARALLEL TO FIBER AXIS: A MODEL CASE OF SEBS WITH
BENZOXAZINE UNDER π - π STACKING CONFORMATION

4.1 Abstract

In our previous work, we declared for the first time an existence of ordered-lamellar microdomains in thermoplastic elastomer based on the case study of the as-spun electrospun polystyrene-b-poly(ethylene-co-1-butene)-b-polystyrene triblock copolymer (SEBS), and also demonstrated how the shear force initiates a certain level of lamellar-microdomain orientation. The present work shows an approach to direct lamellar-microdomain orientation to be parallel to the fiber axis by simply initiating a specific molecular interaction among thermoplastic elastomer chains. The blend system of SEBS and bisphenol-A based benzoxazine monomer (BZ) forms π - π interaction as confirmed by nuclear overhauser effect in nuclear magnetic resonance spectroscopy (NOESY NMR). The electrospun fibers of this blend under a low rotational fiber collector speed (below 310 m/min) show not only the microdomain orientation but also (i) the fragmentation of microdomain to small grains which orient almost perfectly parallel to the stretching direction (SD) or fiber axis, and (ii) the lamellar angles (μ) are also almost parallel to the fiber axis. When rotational collector speed is high enough (~620 m/min, and 1340 m/min), the shear force overcomes the π - π interaction between SEBS and BZ, and as a result, the regular microdomains orientation to the fiber axis are suddenly diminished. Thermal treatment of the fibers at 170 °C initiates the lamellar microdomain rearrangement to an isotropic one with significant traces of lamellar orientation parallel and perpendicular to the fiber axis. The present work demonstrates how two extremely combined conditions which are; (i) macroscopic external stimulus, i.e., stretching force, and; (2) specific interaction at molecular level, i.e., π - π interaction, to direct the orientation of microdomains in the confined space of the as-spun electrospinning fibers to be a uniaxial microdomain aligning parallel to the fiber axis.

Keywords: electrospun fibers, microdomains, π - π interaction SEBS, benzoxazine

4.2 Introduction

Block copolymers is one of polymeric materials which have been extensively studied for decades due to the synergic unique properties, such as toughness, stiffness and chemical resistance, of the different homopolymers.¹⁻³ Morphologically, block copolymers undergo microphase separation spontaneously because of immiscibility of each block. Upon the phase separation, block copolymers form regularly-ordered microdomains, such as spheres,⁴ cylinders,^{5,6} gyroid⁷ and lamellae.⁸ Each microdomain in nanometer scale forms super-lattice structure with the grain which sometime exceeds to tens of micrometers. The unique morphologies play an important role in internal-reinforcement and contributes directly to the macroscopic properties of the materials.⁹ Various techniques, such as annealing¹⁰, applying external forces^{11, 12} and placing in electric field¹³ etc. were used to control microdomain orientation, unification of microdomain grains, etc.

Electrospinning is known as a versatile technique to fabricate ultrafine fiber, in nanometer scale to a few micrometers. Electric force is used to draw the fluid jet from the needle in a milli-second time scale. In other words, the fluid jet is pulled towards the collector with extremely high stress, and solidified into nano- or micro-fibers.¹⁴ Thus, electrospinning is an excellent technique to control microdomain orientation and arrangement since it is not only the technique to give an extremely high stress to the block copolymer fluid, but also restrain the microdomain formation in the confined geometry. Fong and Reneker reported microphase separation of polystyrene-block-polybutadiene-block-polystyrene triblock copolymer (SBS) in the electrospun fibers.¹⁵ However, only ill-developed, small, and peculiar shaped microdomains in the SBS as-spun electrospinning fibers were declared as it might be due to a high evaporation rate of the spinning solvent. It is known that the rapid evaporation of solvent limits polymer chain mobility resulting in segregation into a thermodynamically stable microdomains.^{10, 15-17}

Recently, we declare for the first time an existence of the well-ordered and oriented microdomains in the as-spun electrospinning fibers of block copolymer through the study case of polystyrene-block-poly(ethylene-co-1-butene)-block-polystyrene triblock copolymer (SEBS).¹⁸ The evidences of elliptic and four-spot from 2D-SAXS patterns lead us to a speculation that after the microdomains was formed, they might be deformed by electric force during the spinning resulting in the distorted and fragmented microdomains with the preferential orientation to the fiber axis. It was to our surprise to see that instead of the high rotational disk speed (1 240 m/min), the lower one (31.5 m/min) significantly induced the microdomain distortion. We speculated that the low rotational disk velocity might allow more time for solvent evaporation, vitrification of PS microdomains, and as a result not only an existence of microdomain orientation but also a certain level of orientation parallel to the fiber axis could be generated. In addition, the vitrified PS plays an important role in allowing an effective stretching resulting in a ductile fracture, and in some cases the distorted lamellar structure.

Polybenzoxazines (polyBZ) are reported as a novel type of phenolic resin, which can be prepared from benzoxazine monomers and the consequent thermal curing (Scheme 4.1).¹⁹⁻²⁴ Recently, we showed a unique in-situ nano-sphere polyBZ formation in SEBS film matrices.²⁵ The depth structural analyses brought us to an understanding that initially π - π interaction was formed between aromatic rings of BZ monomer and styrene block in the SEBS chain.

Based on the above mentioned works, it comes to our question about how the π - π interaction between BZ and SEBS play the role in the morphology of SEBS electrospun fiber.

The present work is an extension of our previous work which we successfully showed an existence of microdomain orientation in electrospun thermoplastic elastomer SEBS. Here, we further focus on electrospun SEBS blend with BZ (SEBS-BZ) under two extremely combined conditions which are macroscopic level of electrospinning condition, i.e., stretching force, and molecular level of specific interaction, i.e., π - π interaction between SEBS and BZ to study how

the microdomains of SEBS respond to those conditions, especially when the SEBS are in the form of electrospun under the confined space.

4.3 Experimental

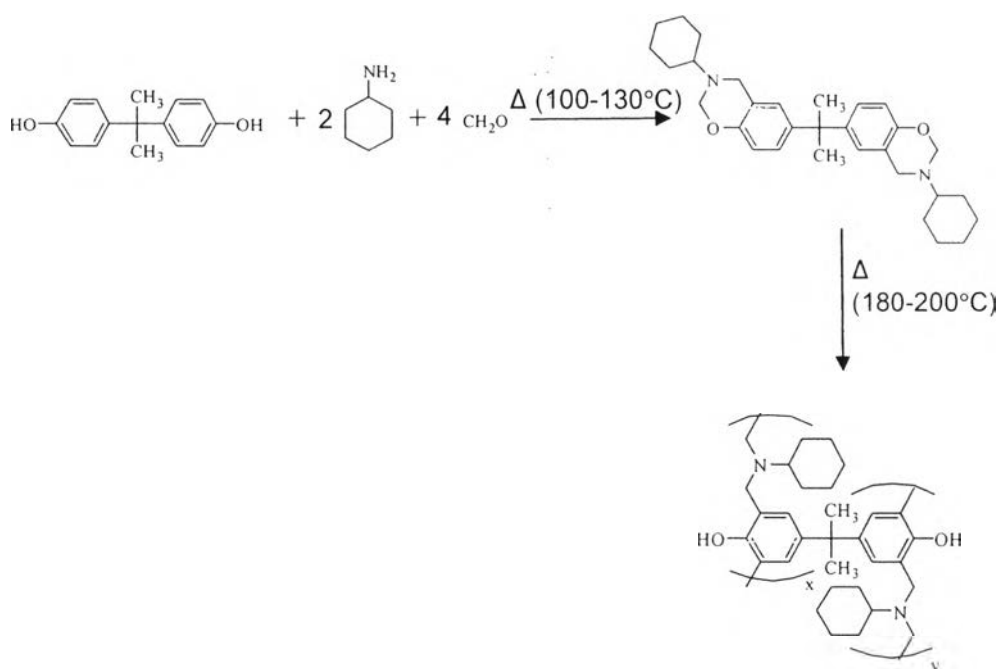
4.3.1 Materials

SEBS triblock copolymer with 32 wt % styrene content, M_w of 77 000 g/mol and M_n of 60 000 with PDI of 1.28, measured by GPC, was provided by Asahi Kasei Chemicals Cooperation, Japan. Bisphenol-A, paraformaldehyde and cyclohexylamine were purchased from Fluka, Switzerland. Chloroform and toluene were purchased from NacalaiTesque, Inc., Japan. All chemicals were used without further purification.

4.3.2 Synthesis of Benzoxazine monomer (BZ).

6,6'-(propane-2,2-diyl)bis(3-cyclohexyl-3,4-dihydro-2H-benzoxazine) was synthesized (Scheme 4.1) from bisphenol-A, formaldehyde and cyclohexylamine by mixing and stirring at about 110°C for 30 minutes as reported elsewhere.²⁰

Scheme 4.1 Synthesis of cyclohexylamine-based bisphenol BZ and its curing reaction to polyBZ



4.3.3 Preparation of SEBS-BZ blending electrospun fibers.

SEBS and BZ were mixed in a weight ratio (wt/wt) of 75:25 (S75BZ25). The mixture was dissolved in the mixed solvent of chloroform/toluene (80/20 wt/wt). The homogeneous solution obtained was electrospun by using a Nanon Electrospinning Setup (MECC Co., Ltd., Japan) equipped with an originally designed rotational disk collector. The optimal spinning conditions were: accelerated voltage, 20 kV; volumetric flow rate, 0.5 mL/h; and, tip-to-collector distance, 15 cm. The fibers were collected onto a rotational disk collector with controllable take-up velocity (i.e., 31.5 m/min, 310m/min, 620 m/min and 1240 m/min). The relative humidity for spinning was in the range of 30-32 %..

4.3.4 Characterizations

Two-dimensional nuclear magnetic resonance (2D-NMR) in nuclear overhauser effect spectroscopy (NOESY) mode was conducted by an NMR BrukerUltrashieldPlus 500 MHz at room temperature with a mixing time of 0.4 second. The fiber morphology was observed by a JEOL JSM-5200 scanning electron microscope, and the average fiber diameter was determined by Image J software. 2D-SAXS measurements were carried out at the RIKEN structural biology beamline I (BL45XU) SPring-8, Hyogo, Japan. The 2D-SAXS patterns were recorded by using a RIGAKU R-AXIS IV++ equipped with an imaging plate detector (300 mm x 300 mm area). The X-ray wavelength, λ , was tuned at $\lambda = 0.10$ nm, and q value, defined by $q = (4\pi/\lambda)\sin(\theta/2)$ (θ : the scattering angle), was calibrated by chicken tendon collagen having the spacing of 65.3nm. The viscosity of the spinning solutions were measured by a Brookfield viscometer (Model DVIII, Brookfield Engineering Labs INC., Stoughton, MA, USA) with temperature control at 28 °C.

4.4 Results and Discussion

π - π Interaction between BZ and PS block in SEBS

Figure 4.1 shows a 2D-NMR NOESY spectrum of S75BZ25 in CDCl_3 . The aromatic protons of BZ are seen clearly at the chemical shifts of 6.97, 6.82 and 6.68 ppm which contribute to the aromatic proton of BZ in the position 3, 1 and 2, respectively. The proton resonance of PS can be observed as a broad peak in the range of 6.97 – 7.24 ppm. The NOESY spectrum clearly shows a correlation between the aromatic proton of BZ at position 2 (H_{BZ2}) and that of PS in SEBS. This implies π - π interaction which might be formed either by charge transfer between electron-rich and electron-poor aromatic compounds^{26,27} or by local dipole of charge distribution in identical-electronic aromatic compounds^{28, 29}. The later maybe appropriate for our case since both aromatic rings in the BZ and in the PS block are electron-rich type.

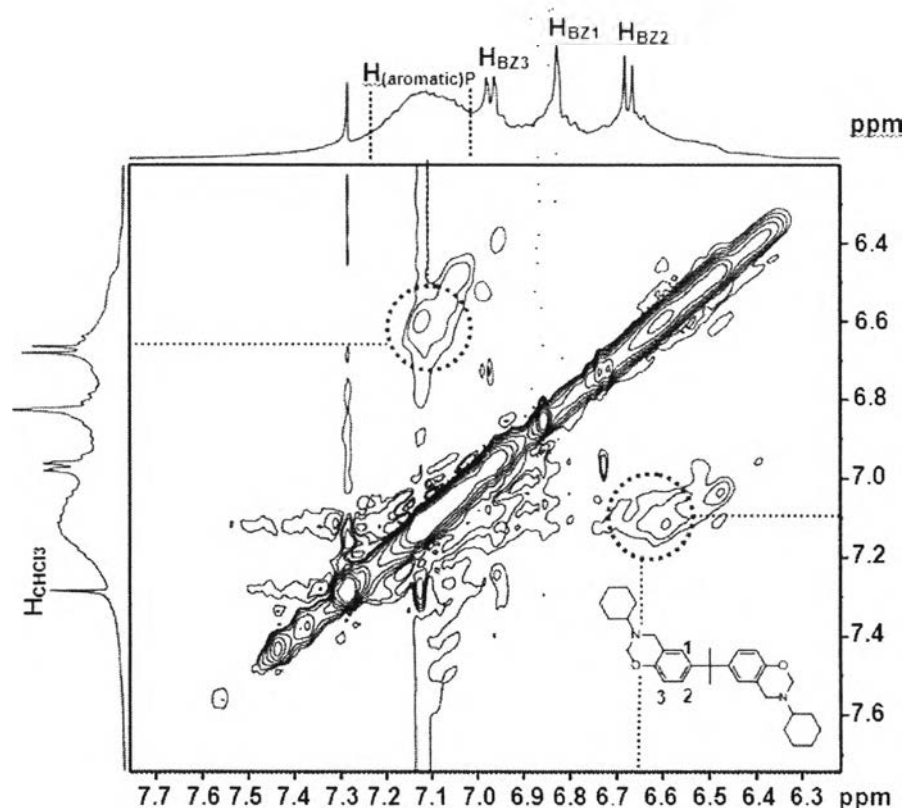


Figure 4.1 2D-NMR NOESY contour plot of S50BZ50 in CDCl_3 at concentration of $3.9 \times 10^{-3}\%$ w/w

DSC thermograms of SEBS and the S85BZ15, and S75BZ25 films are shown in Figure 4.2. The T_g of PEB segment at around -60°C can be distinguished as the position A. An endothermic-broad peak at around 70°C (position B) belonging to an enthalpy relaxation of polystyrene near $T_g^{30, 31}$ is also identified. The enthalpy relaxation is confirmed from the fact that this peak can be observed only in the first-heating scan. As this peak is related to which the effect of BZ on PS segment chain relaxation, a careful observation gives us important information of the interaction with BZ. It is clearly seen and specially considered. The enthalpy relaxation of the as-cast SEBS film is 0.56 J/g . In the case of SEBS-BZ, it is clear that an increase of BZ content leads to an increase of enthalpy relaxation value. For example, the value is as high as 2.17 J/g and 2.32 J/g for S85B15 and S75BZ25 films, respectively (Figure 4.2). This implies how PS blocks were in constrained by BZ. In other words, PS blocks are in less favorable state or less entropic state. The behavior of SEBS/BZ in DSC thermogram reflects the π - π interaction between SEBS and BZ.

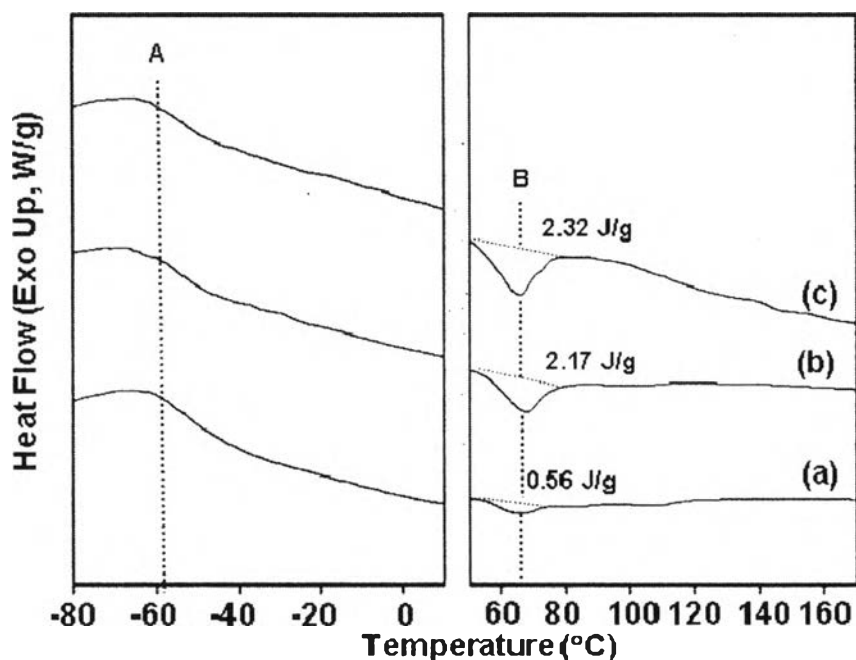
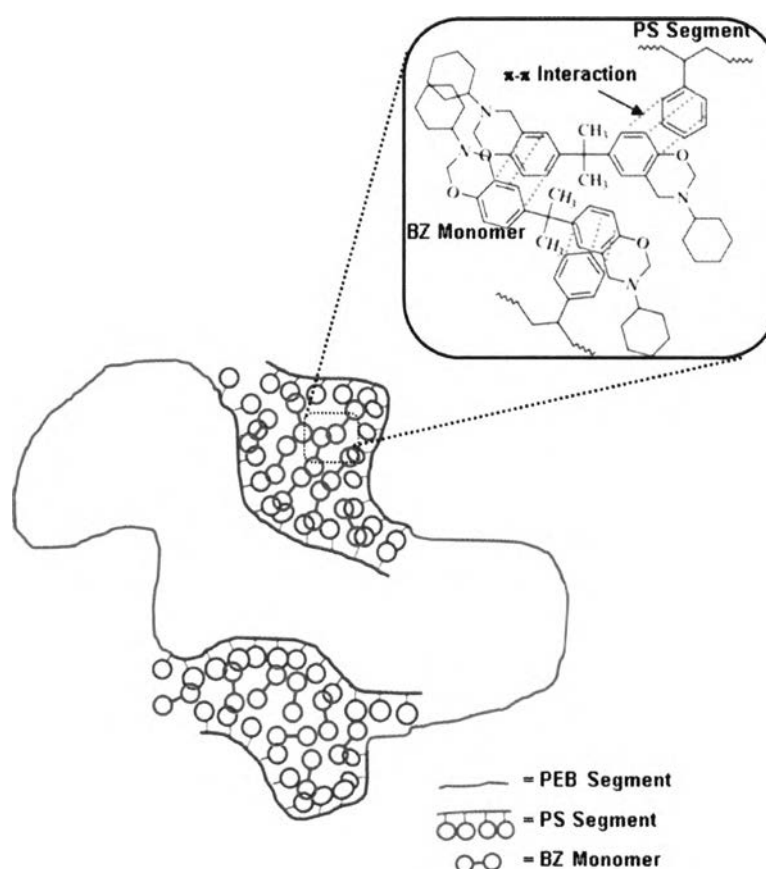


Figure 4.2 DSC thermograms of : (a) SEBS film, (b) S85B35 film and (c) S75BZ25 film.

Viscosity of spinning solutions were found to increase significantly from 1449 cp (± 4 cp) for SEBS to 1743 cp (± 3 cp) for S75BZ25 under the same concentration of 18 %wt. The fact that the mixture showed an increase in viscosity in spite of the actual concentration of SEBS was diluted by adding BZ for 25 %wt, this further confirms us the π - π interaction between SEBS and BZ as shown in Scheme 4.2

Scheme 4.2 Suspected mechanism for vitrification of PS segments via π - π interaction between aromatic rings of BZ and PS in SEBS chains



Microdomain structure of SEBS film

In order to investigate the structural change of microdomains in the as-spun fibers, their morphology in an equilibrium state (film state) should be first clarified.

Thus, as-cast film SEBS was characterized by 2D-SAXS to find that it shows a series of scattering maxima at relative q positions of 1: 2: 3: 4 suggesting a lamellar morphology of the microdomains (Figures 4.3 (a) and (c)). For the S75BZ25 film, Figure 4.3(b) shows a series of scattering maxima at relative q positions similar to that of as-cast SEBS film indicating lamellar-microdomain structures. Furthermore, the circular patterns (Figures 4.3(c) and (d)) indicate a certain level of isotropic orientation of lamellar microdomains in both as-cast SEBS and S75BZ25 films. It should be noted that S75BZ25 film shows a slight decrease of each q position. This means that there is a slight increase of lamellar repeating period, as compared to SEBS film. The increases in lamellar period might be accounted for an occupation of BZ in PS lamellar microdomains.

The DSC thermograms in Figure 4.2 also support our speculation. The T_g s belonging to PEB block for SEBS, S85BZ15 and S75BZ25 appear at the same temperature, i.e., at -60 °C, whereas the chain relaxation temperatures of PS blocks for SEBS, S85BZ15 and S75BZ25 appear in the order of $S75BZ25 > S85BZ15 > SEBS$.

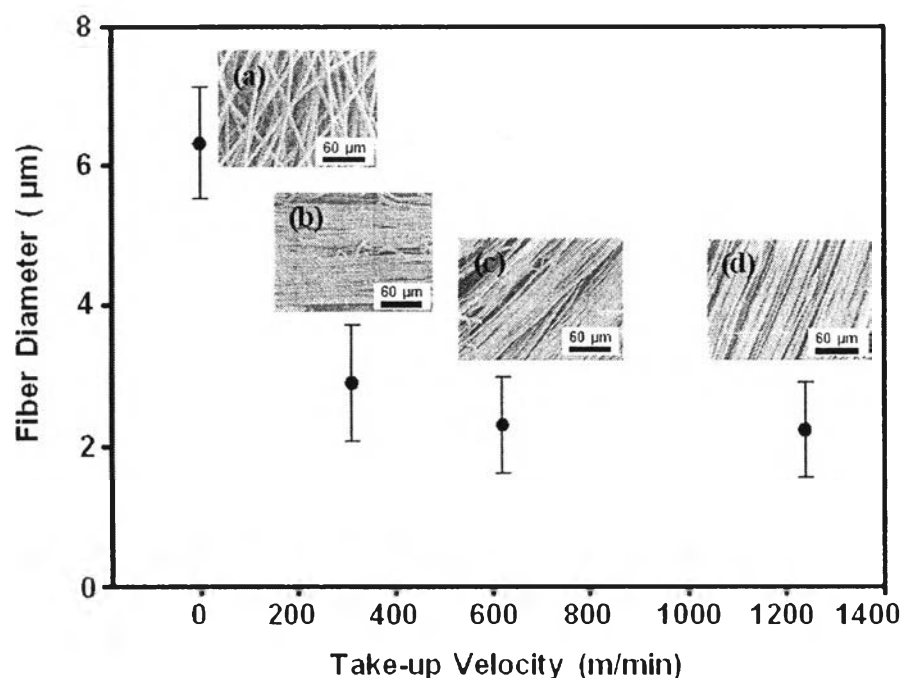


Figure 4.3 Fiber diameters of as-spun S75BZ25 electrospinning fibers at various take-up velocities including their SEM images; (a), (b), (c) and (d) for those fibers collected at 0 m/min, 310 m/min, 620 m/min, and 1240 m/min, respectively.

Microdomain arrangement and orientation of as-spun SEBS fibers

The optimal electrospinning parameters were preliminary studied to find the conditions as follows; accelerate voltage at 20 kV, 18 wt% solid content of SEBS in the mixed solvent (80:20/chloroform: toluene). In order to investigate the effect of shear force to microdomain arrangement and orientation in SEBS electrospun fibers, the rotational disk collector velocities were varied from 31.5 m/min to 1 240 m/min. Figure 4 shows the appearances and sizes of the fibers as observed by SEM. The plots of fiber diameters indicate clearly how the take-up velocity significantly reduced the fiber diameter. The minimum diameter is about 2.5 μm which belongs to the fibers obtained from the rotational disk collector speeds at 620 m/min and 1240 m/min. This suggests that the high stretching force initiated by the high take up velocity of rotational disk collector leads to a decrease in fiber diameters. As discussed in our previous work, the viscoelasticity and low conductivity of the spinning solution limited us to obtain the fiber diameter smaller than 1 μm .

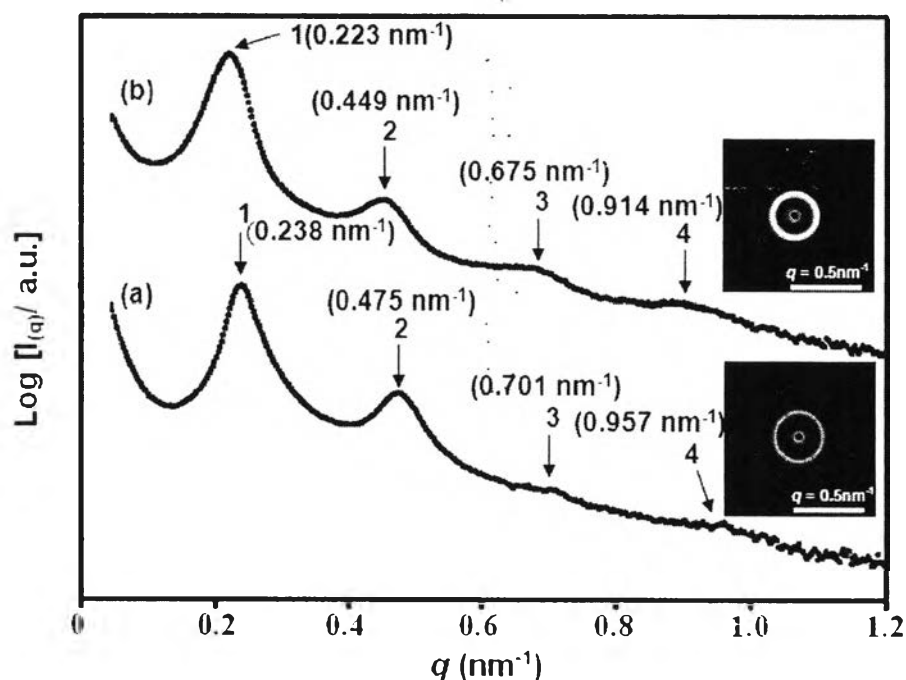


Figure 4.4 Circular average SAXS profiles of (a) SEBS film and (b) S75BZ25 film including their 2D-SAXS patterns of (c) SEBS film and (d) S75BZ25 film.

Microdomain structure of as-spun SEBS fibers

Previously we already clarified an existence of short-order lamellar microdomains and their orientation.¹⁸ Here, the detailed analyses relevant to rotational disk collector speed or fiber take-up velocity of SEBS microdomains are done.

Figures 4.5 (a) and (b) summarize the 2D-SAXS patterns of the SEBS electrospun which elliptic and four-point patterns are identified. The elliptic pattern refers to the distorted microdomains as a result of stretching force during spinning along the fiber axis, whereas the four-point pattern is ascribed to glassy lamellar microdomains which are ruptured to tiny fragments, so-called herringbone structure.³² It should be emphasized that the four peaks were aligned obliquely to the SD upon uniaxial stretching.^{9,33} At that time, the fibers collected at the lowest (31.5 m/min) take-up velocity show the most distorted lamellar microdomains. This unexpected result could be related to vitrification of PS microdomains. The vitrification is depending on the time for solvent evaporation. The stretching of the fiber with vitrified PS microdomains might lead to the highly distorted lamellar structure as Figure 4.5 (c).

Effect of BZ on microdomains of SEBS

As BZ forms a kind of physical crosslink with PS segments in SEBS via π - π interaction, here it comes to our question about how this physical crosslink initiates the change in morphology. The changes of microdomains in the as-spun electrospinning SEBS fibers under the effect of BZ can be traced by 2D-SAXS patterns. Here, to simplify the study only the SEBS blend with BZ for 25 %wt content (S75BZ25) was considered.

The structural change of the microdomains in as-spun SEBS and S75BZ25 fibers upon an increase of take-up velocity was qualitatively analyzed as follows. The as-spun SEBS shows dark streaks along equatorial direction (Figure 4.5 (a)). The as-spun S75BZ25 obtained from any take-up velocities also shows the dark streaks (Figure 4.5 (d), (g), (j) and (m)) similar to the case of the as-spun SEBS. This indicates a lack of lamellae that aligns perpendicular to the fiber axis which was

discussed in our previous work.¹⁸ A careful observation on the scattering patterns of the as-spun SEBS fibers leads us to see pattern I (elliptical pattern) and pattern II (four-spot or four-streak pattern) as quoted in Figure 4.5 (b). The elliptical pattern reflects the distorted-lamellar microdomains which might come from the stretching stress as simplified in Figure 4.5 (f) whereas the four-spot pattern refers to the fragmented lamellar structure as illustrated in Figure 4.5 (c). (see Microdomain structure of as-spun SEBS fibers)

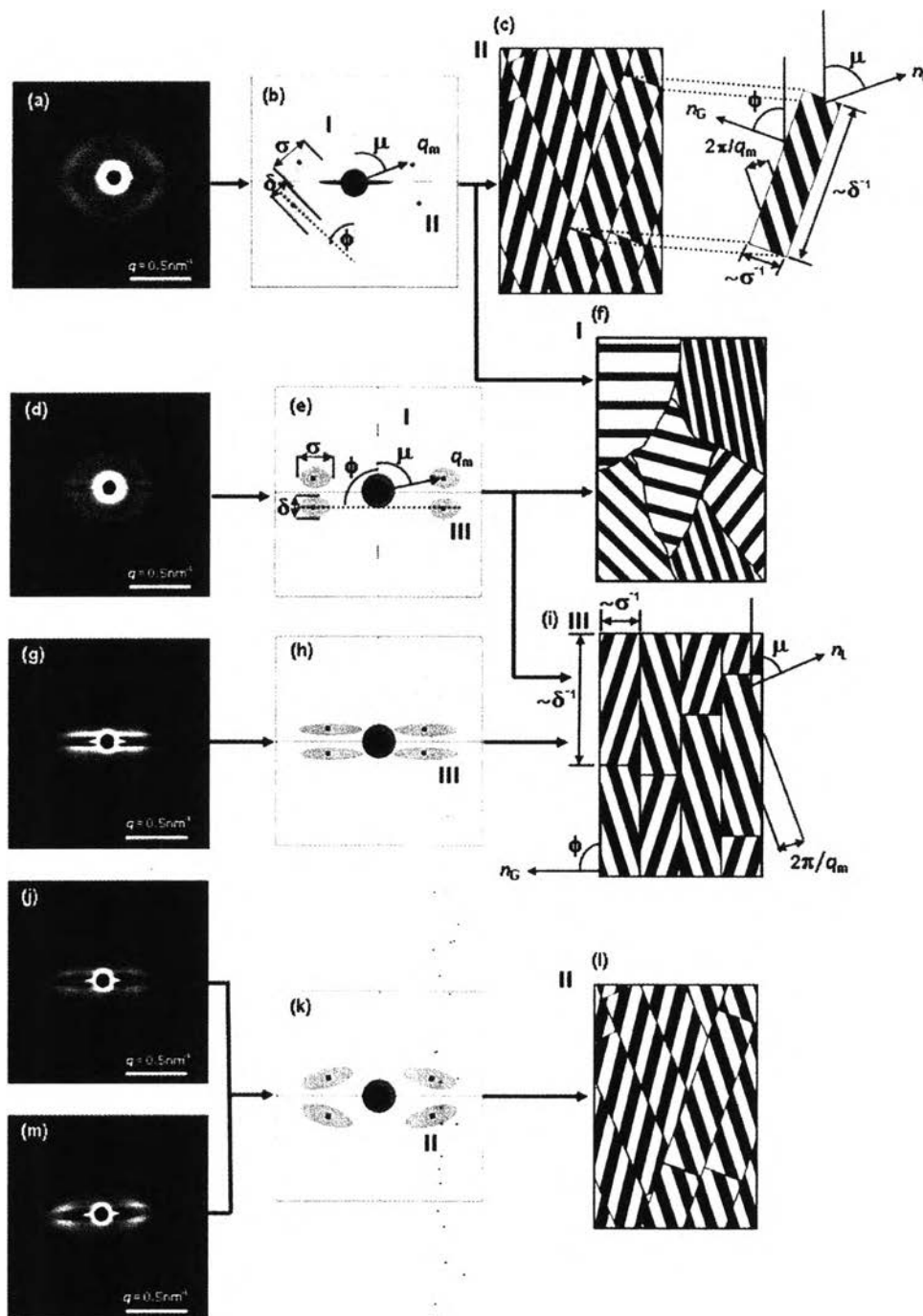


Figure 4.5 2D-SAXS patterns of (a) as-spun SEBS electrospinning fibers collected at 310 m/min, and as-spunS75BZ25electrospinning fibers collected at : (d) 31.5 m/min, (g) 310 m/min, (j) 620 m/min and (m) 1240 m/min. (b), (e), (h) and (k) are schematic illustrations highlighting the features of the 2D-SAXS patterns of (a), (d), (g)and (j), respectively. (f), (c) and (i); and (i) are possible models to represent (I) distorted-lamellar, (II) oblique-herringbone and (III) parallel-herringbone structure, respectively.

In the case of S75BZ25 fibers collected at the lowest take-up velocity, i.e. 31.5 m/min, both elliptical pattern and four-spot pattern are identified (Figure 4.5 (d)). It is important to note that the ϕ angle of the four-spot peak is found to be 90° to the fiber axis. This indicates that the lamellar grains are oriented in parallel to the SD. When the stretching was varied by increasing the rotational disk collector speed, for example to 310 m/min, the four-spot pattern becomes obvious and the elliptical peak is diminished. This implies that at this level of the stress, the large distorted microdomain grains are ruptured to tiny ones and oriented obliquely to the stretching direction. Figure 4.5 (i) and (l) simplify the structure as assets of herringbones to represent the ruptured grains.

Taking the above results into our consideration, we suspect the microdomain formation of S75BZ25 as follows. Based on the physical crosslink between BZ and PS block in SEBS chain under π - π interaction, the spinning solution ejected from the needle PS microdomains were more or less vitrified. At that time the vitrified PS was well responsive to the external force, i.e., stretching force from rotational disk collector. This brought a significant microdomain distortion which never appeared in pure SEBS case.

In order to characterize the herringbone structure in details, each parameter from 2D-SAXS patterns was extracted and evaluated (Figures 4.5 (b) and (e)).³⁶ As the imperfection in symmetry may cause some differences in each streak-like spot, each parameter was averaged to obtain a representative value. For fibers collected at take-up velocities of 31.5 m/min and 310m/min as illustrated in Figures 4.5 (e) and (h), the four streaks are parallel to each other and perpendicular to the fiber axis as can be written as pattern III. The pattern III refers to the anisotropic lamellar -under the shaped grains orient longitudinally parallel to the fiber axis as schematic drawn in Figure 4.5 (i). The widths of the streak in perpendicular and parallel direction to the fiber axis are assigned to parameters σ and δ , respectively, as indicated in Figures 4.5 (b) and (e). The inverse proportional to the grain size and the direction perpendicular and parallel to the fiber axis are also shown in Figure 4.5(c) and (i). The angle parameters, ϕ and μ , are for an oblique angle of the streak with respect to the fiber axis and for an angle between the q vector pointing to the peak maximum and the

fiber axis, respectively (Figure 4.5 (b) and (e)). According to the herringbone structure, ϕ and μ are corresponding to the angles normal vectors of the grain, n_G , and to the lamellar microdomain, n_L , with respect to the fiber axis, respectively (Figure 4.5 (c) and (i)). The magnitude of q vector at the peak maximum is denoted by q_m , which is inversely proportional to the lamellar repeating period. For the fibers collected at 620 m/min and 1240 m/min, the four streaks are obliquely oriented to the fiber axis as pattern II (Figures 4.5 (j) and (m)) as in Figure 4.5 (k).

Microdomain Parameters

Figure 4.5 contains important information for quantitative analysis of microdomain orientation. Here, each parameter, i.e., lamellar repeating period ($2\pi/q$), grain dimension (δ , and σ), grain tilt angle (ϕ), and lamellar tilt angle (μ), were analyzed and calculated based on the 2D-SAX results in Figure 4.5.

For lamellar repeating period (Figure 4.6 (A)), in the case of SEBS fibers, the values are almost constant (about 17-18 nm) for all fibers obtained from different take-up velocities. This implies that the take-up velocity does not affect the lamellar of SEBS. However in the case of S75BZ25, the lamellar repeating periods are about 20-25 nm which are larger than those of SEBS. The S75BZ25 fiber obtained from the take-up velocity 310 m/min shows the highest lamellar repeating period. Although the reason is not clear to us, the fact that this take-up velocity gives the most microdomain orientation parallel to the fiber axis, we assume that this velocity is a critical velocity that π - π interaction still effectively maintained (see further discussion in Figure 4.6 (B), and (C))

The σ and δ values (Figure 4.6 (B)) are relevant to the grain dimension. For comparative information, the σ and δ values, which can be roughly approximated to be the width and length based on $2\pi/q$, were considered. In the case of SEBS, the grain dimension based on σ values (0.28 - 0.34 nm⁻¹) and δ values (0.09 - 0.12 nm⁻¹) could be referred to the width and length of 18-20 nm and 51-75 nm, respectively. This indicates that although the take-up velocity was varied, the changes of the grain dimension are not significant.

In the case of S75B25, the σ values (0.24-0.28 nm⁻¹) and δ values (0.04-0.08 nm⁻¹) could be referred to the width and length of about 22-26 nm and 80-150 nm, respectively (Figure 4.6 (B)). The take-up velocities at 310 m/min initiate the length of the grains to be the highest which is 150 nm. This implies (i) the take-up velocity did not have the effect on the width (σ) as much as on the length (δ), and (ii) a certain level of take-up velocity initiates the longest grain of lamellae.

It is important to note that both parameters, σ and δ , of S75BZ25 are smaller than those of the as-spun SEBS, in other words, the lamellar microdomains of S75BZ25 are relatively larger than those of the as-spun SEBS. This might come from the more vitrified microdomains due to the π - π bonded network between BZ and PS segments in SEBS.

The ϕ and μ values allow us to consider how the SEBS fibers align to the SD. The ϕ values maintain at 78-80° for all take-up velocities (Figure 4.6 (C)). The ϕ values of SEBS fibers are about 50° for all take-up velocities whereas those of S75BZ25 are varied. The take-up velocities at 31.5 and 310 m/min give the ϕ values for 105°. This indicates a parallel directing of lamellar grains to the SD. The ϕ values abruptly drop to 78° when the take-up velocity is above 310 m/min. For μ values, those of SEBS are maintained at about 60° whereas those of S75B25 are maintained at about 80°. It should be noted that both angle parameters, μ and ϕ , are higher than those of SEBS fibers for all take-up velocities. As compared to the SEBS fibers, S75BZ25 shows lamellar microdomains and microdomain grains directing parallel to the fiber axis or SD.

Corresponding to those parameter changes upon increase the take-up velocity (in other words, increase the stretching force) the change of the microdomains in real space can be concluded as follows. In the case of S75BS25 fibers, at low take-up velocity, i.e. 31.5 m/min, the internal structure was stretched resulting in distortion of lamellar grains and some parts were fractured into large fragmented-lamellar grains, showing the longest of grain length (the lowest σ value), and the orientation parallel to the SD. As the stretching force increased, the distorted and large fragmented grains are fractured to tiny ones but still in an orientation

parallel to the SD as evidenced from the $\phi = 90^\circ$ for the take-up velocity at 310 m/min).

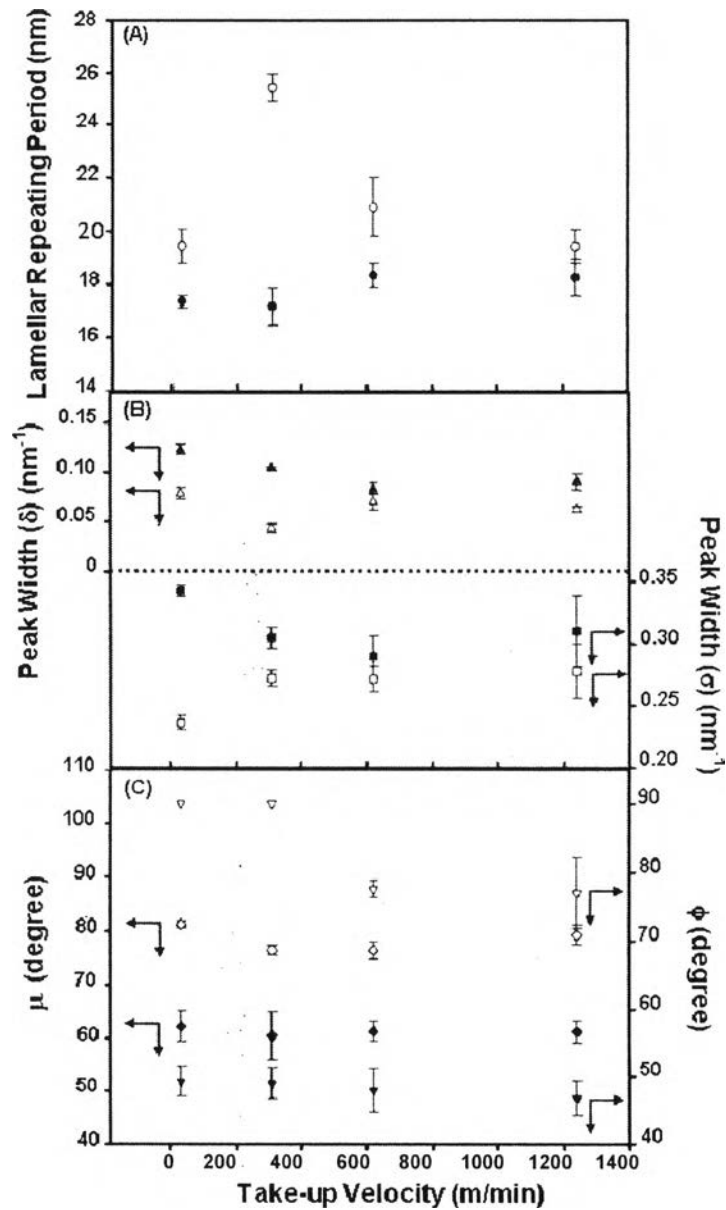


Figure 4.6 Structural parameters of as-spun electrospinning fibers collected at various take-up velocities: lamellar repeating periods of SEBS (\bullet) and S75BZ25 (\circ); peak width parameters σ and δ of SEBS (\blacktriangle) and (\blacksquare), and S75BZ25 (\triangle) and (\square); angle parameters μ and ϕ of SEBS (\blacklozenge) and (\blacktriangledown) and S75BZ25 (\triangledown , (\diamond), respectively.

To examine the individual grain more concretely, other three parameters, i.e., persistence length of the fragmented lamellae (l_p), packing angle (α), and number of the packed lamellae in the grain (m) (Figure 7) were considered. Their geometrical definitions are expressed as the following equations³⁶

$$l_p = k \left[\sigma \cos \left(\mu + \phi - \frac{\pi}{\nu} \right)^{-1} \text{ for } \alpha \geq \tan^{-1} \left(\frac{\delta}{\sigma} \right) \right]; \text{ (k is arbitrary constant)} \quad (1)$$

$$l_p = k \left[\delta \cos \left(\mu + \phi - \frac{\pi}{\nu} \right)^{-1} \text{ for } \nu < \tan^{-1} \left(\frac{\delta}{\sigma} \right) \right] \quad (2)$$

with

$$\alpha = \pi - (\mu + \phi) \quad (3)$$

, and

$$m = k q_m (\sigma^{-2} + \delta^{-2})^{1/2} \cos \left[\alpha + \tan^{-1} \left(\frac{\delta}{\sigma} \right) - \frac{\pi}{2} \right] \quad (4)$$

To simplify the calculation, k was assumed to be unity, and the calculated parameters are shown in Figures 4.7. In the case of SEBS fibers, both l_p and α values are consistent for all take-up velocities. For S75B25 fibers, the l_p values are about 8-16 nm which are 4-6 times higher than that of SEBS. It is important to note that the l_p values are significantly high at the low take-up velocity until 310 m/min and decreases afterward. In contrast, the α values are small at the low take-up velocity and increases with an increase of the take-up velocity. The α values of S75BZ25 fibers are smaller than that of SEBS fibers in all take-up velocities suggest that the longitudinal-axis direction of the lamellar microdomains (l_L) orients in closer angle to the longitudinal-axis direction of the lamellar grains (l_G) in S75BZ25 fibers than that in the SEBS fibers. The low α angles emphasize that the S75BZ25 lamellar microdomains and their grains are parallel to the fiber axis or SD. As shown in Figure 4.7 (D), the concrete image regarding to l_p and α is that each grain of S75BZ25 consists of the very long but little tilt lamellar.

Figure 4.7 (C) declares the number of the packed lamellar of S75BZ25 is fewer than that of SEBS for all take-up velocity. This implies that in a certain value containing SEBS and BZ, the lamellar microdomain might be occupied by the BZ, in

other words, the SEBS might give the larger lamellar repeating period resulting in the small amount of the number of the packed lamellar.

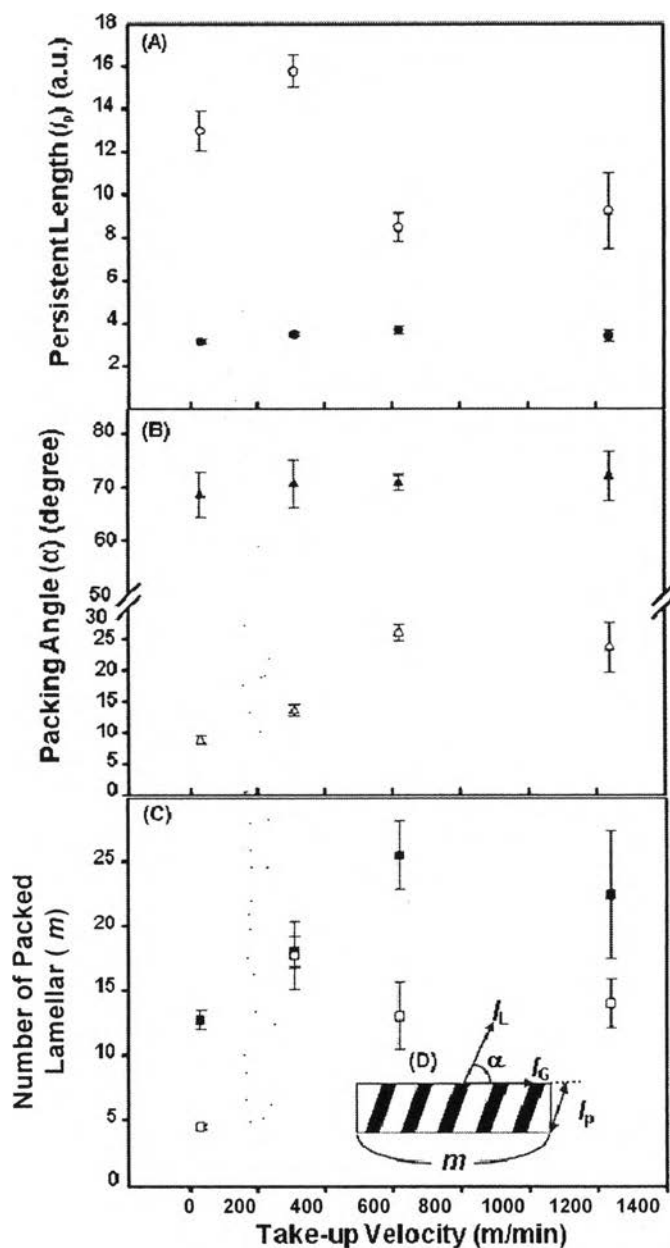


Figure 4.7 Persistence length of the fragmented lamellae (l_p), packing angle (α) and number of the packed lamellae in the grain (m), where arbitrary constant (k) in equation (1), (2) and (4) was assumed to be unity, of SEBS (\bullet), (\blacktriangle) and (\blacksquare); and S75BZ25 (\circ), (Δ) and (\square) as-spun electrospinning fibers, respectively, collected at various take-up velocities

Critical Level of Molecular Interaction in Responsive to Fiber Stretching

Here, another important point is needed to be clarified. As illustrated in Scheme 4.2, the π - π interaction plays an important role in forming physical crosslink network between SEBS and BZ during fiber spinning. It comes to our question that at what level that the stretching force overcomes this interaction. As the stretching force can be controlled by the fiber take-up velocity, the velocity was further increased to observe the change of microdomain. Figure 4.5 (j) shows that when the S75BZ25 was collected at the velocities of 620 m/min and 1 240 m/min, the oblique four-streak pattern is observed again. In other words, the 2D-SAXS patterns become similar to that in the as-spun SEBS fibers (Figure 4.5 (a)).

Figure 4.6 also confirms how the applied force obtained from the high take-up velocities, i.e. 620 m/min and 1 240 m/min affects the physically bonded network between BZ and SEBS. For example, the lamellar repeating period, and the δ and σ values become close to those of SEBS when the take-up velocities are 620 m/min and 1 240 m/min. In fact, at those velocities, the ϕ angles also disrupt from 90° suggesting a significant disorientation of the lamellar grain respecting to the fiber axis (Figure 4.6 (c)). The results obtained from Figure 4.7 indicate the grain details become similar to those of SEBS.

Comparative Microdomain Orientation between SEBS and S75BZ25

To simplify the discussion on microdomain orientation, the models highlighting a single grain of lamellar microdomains are schematically drawn based on the 2D-SAXS results (Figure 4.8). For S75BZ25 fibers collected at 31.5 m/min, the stretching initiated a preferential orientation of the grain to be almost parallel to the fiber axis as well as the lamellar orientation. For the take-up velocity of 310 m/min, although the grains are still oriented parallel to the fiber axis, the grains are fractured to the smaller ones as compared to those of the fibers collected at 31.5 m/min.

When the take-up velocity becomes higher (610 m/min, and 1240 m/min), the orientation of the grain and the lamellae became loose as evidenced from the oblique orientation in 2D-SAXS patterns. The packing of the lamellae became

similar to that of the SEBS fibers. Thus, it seems that there is a critical level in between 310 m/min and 620 m/min of the disk collector speed to overcome the parallel orientation of S75BZ25 to be shifted from the fiber axis. In other words, (i) the optimal rotational disk speed to direct microdomain orientation of S75BZ25 fiber to the fiber axis is about 310 m/min, and (ii) at the rotational disk speed more than this, the π - π interaction between SEBS and BZ in S75B25 might be weakened and as a result, the microdomain orientation became significantly shift from the fiber axis and became close to the ordinary SEBS.

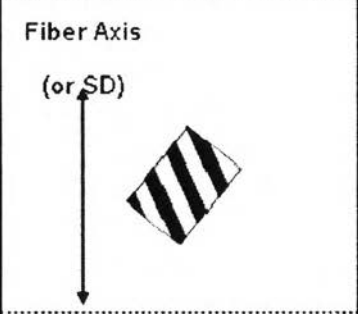



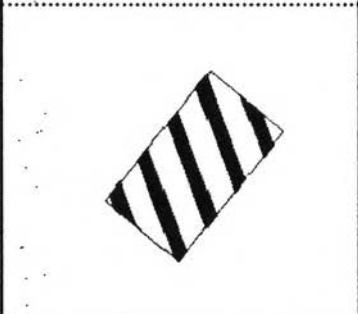

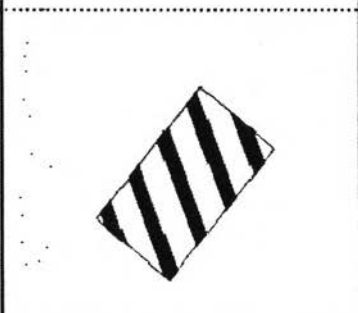

Take-up Velocity	SEBS As-spun Electrospinning Fibers	S75B25 As-spun Electrospinning Fibers
31.5 m/min	Fiber Axis (or SD) 	
310 m/min		
620 m/min		
1240 m/min		

Figure 4.8 Schematic illustrations showing the changes of lamellar microdomain orientation, representing in individual grain, of SEBS and S75BZ25 as-spun electrospinning fibers at various take-up velocities. Note that these are quantitatively based on structural parameters evaluated from 2D-SAXS patterns.

Rearrangement of Lamellar Microdomains in S75BZ25 Fibers under Thermal Treatment

As reported by Ma et al. and Kalra et al., the peculiar shape microdomains of poly(styrene-block-isoprene) (SIS) electrospun fibers show a rearrangement to a long-ranged ordered ones, as observed in film, after a thermal annealing.^{8, 10, 17} In our previous work¹⁸, we showed that the oblique-oriented lamellar microdomains of the as-spun SEBS electrospun fibers performed the rearrangement to the randomly-oriented lamellar ones with dually preferential directions, parallel and perpendicular to the SD by the annealing. However, it should be noted that those preferential orientations of the long-ranged microdomains were observed only in the fibers collected at high take-up velocities (610 and 1 240 m/min) although the as-spun fibers collected at the lowest take-up velocity (31.5 m/min) showed the most distorted lamellae. Thus, it comes to the question how the highly-oriented lamellar microdomains in the as-spun S75BZ25 fibers rearrange themselves by thermal treatment.

The fibers were fixed by epoxy glue before annealing at 170°C for 3 hours to maintain the fiber structure as original ones. Figure 4.9 (A) shows 1D-SAXS profiles (circular average of 2D-SAXS patterns) of annealed S75BZ25 fibers including the films of SEBS and S75B25 for comparative discussion. The as-cast SEBS films show the lamellar repeating period for ~26.6 nm (profile (a)). The S75BZ25 films before curing show the lamellar repeating period for ~28.1 nm (profile (b)) which confirms the occupation of BZ in the lamellar microdomains. After this film was cured, the lamellar repeating period decreases to ~24.3 nm (profile (c)). This suggests a removal of remaining strain based on the thermal treatment. In the case of S75B25 fibers, (profiles (d)-(f)), the lamellar periods of all fibers appear at the same position at ~21.9 nm. This indicates the tight lamellar period as compared to that of the films.

Figure 4.9 (B) shows 2D-SAXS patterns for the annealed S75BZ25 fibers which were collected at the varied take-up velocities. It is clear that the microdomain relaxations of all fibers were formed resulting in the isotropically symmetrical ring. This suggests that the fragmented-lamellar microdomains reorganize to a favorable

random morphology according to SEBS chain relaxation. Moreover, it should be noted that the preferential orientation of lamellar microdomains after curing is discernible as referred to the intensity accumulation on both equatorial and meridional directions for the first-order peak (arrows in Figure 4.9 (B)).

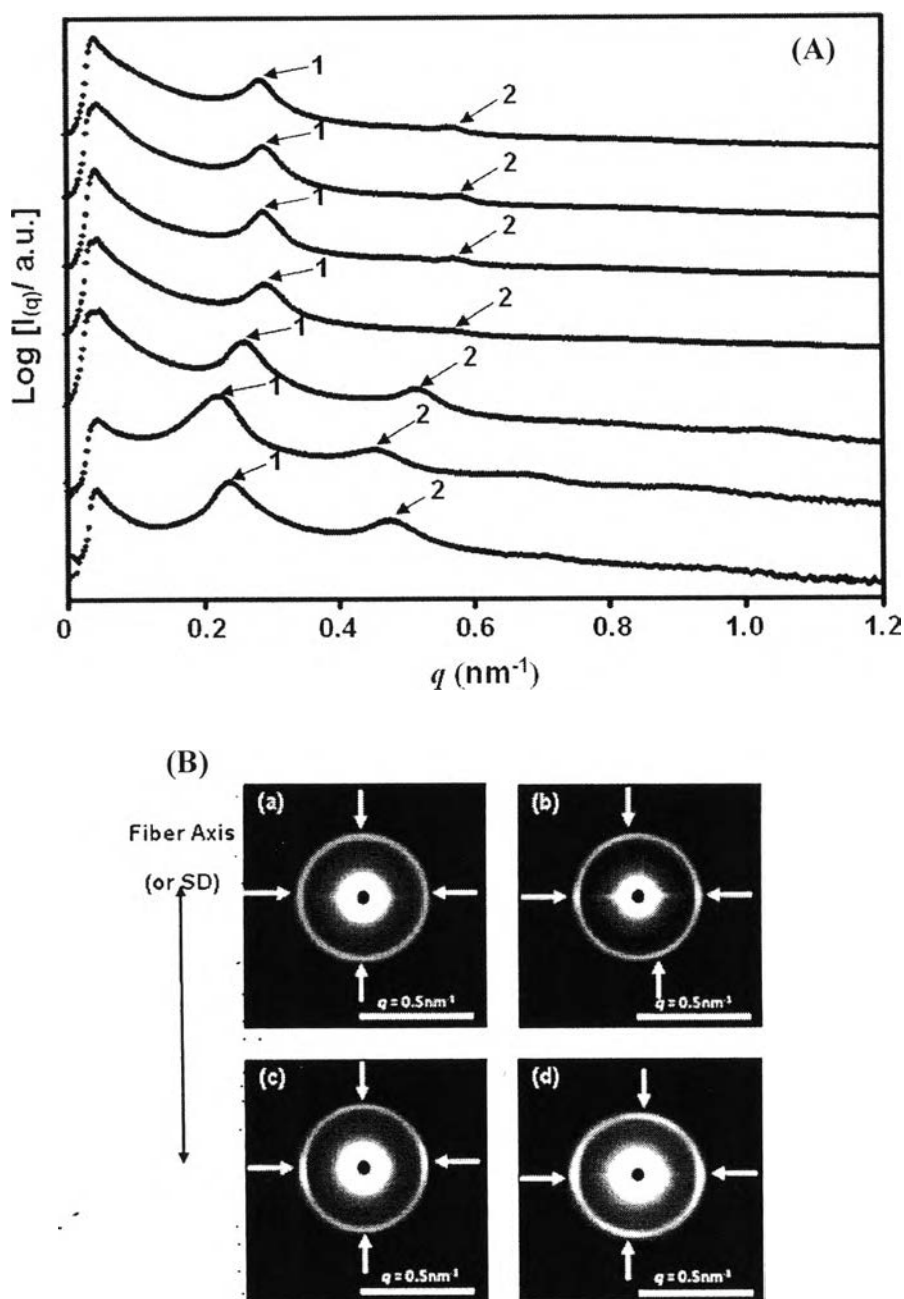


Figure 4.9 (A) 2D-SAXS patterns of the post-cured S75BZ25 electrospinning fibers collected at : (a) 31.5 m/min, (b) 310 m/min, (c) 620 m/min and (d) 1240 m/min, and (B) SAXS profiles of : (a) as-cast SEBS film, (b) pre-cured S75BZ25 film, (c) post-cured S75BZ25 film and post-cured S75BZ25 electrospinning fibers collected at : (d) 31.5 m/min, (e) 310 m/min, (f) 620 m/min and (g) 1240 m/min. The fibers were fixed in adhesive epoxy before curing at 170°C for 3 hours.

To clarify the intensity accumulation, the intensity distributions with azimuthal angle (φ) were scanned (Figure 4.10 (A)). The accumulated intensities in parallel direction (equatorial direction), i.e. $\varphi_{90^\circ, 270^\circ}$, and perpendicular direction (meridional direction), i.e. $\varphi_{0^\circ, 180^\circ}$, to the SD are observed. The annealed fibers collected at 310 m/min, 620 m/min, and 1240 m/min, show the significant accumulated intensity at $\varphi_{90^\circ, 270^\circ}$ rather than those at $\varphi_{0^\circ, 180^\circ}$. This indicates that, during the annealing, the stress stored in the SEBS chains was released. Consequently, it induces the long-range ordered microdomains preferentially oriented in the SD. To concretely evaluate the microdomain orientation, a Herman's orientation function (f) was calculated from the following equations:

$$f = \frac{[3\langle \cos^2 \varphi - 1 \rangle]}{2} \quad (5)$$

and,

$$\langle \cos^2 \varphi \rangle = \frac{\int_0^{\frac{\pi}{2}} I_{(\varphi)} \cos^2 \varphi \sin \varphi d\varphi}{\int_0^{\frac{\pi}{2}} I_{(\varphi)} \sin \varphi d\varphi} \quad (6)$$

The f value is unity in the case of perfectly parallel orientation of lamellar microdomains, and is -0.5 in the case of lamellae oriented perfectly perpendicular to the fiber axis. In the case of randomly lamellar orientation, the f value is nearly zero. However, in our case, the patterns show dually accumulated-intensity directions. Thus, the $f_{90^\circ, 270^\circ}$ and $f_{0^\circ, 180^\circ}$ were separately calculated in the range of 50-125° and 230-320° for $\varphi_{90^\circ, 270^\circ}$, and of 125-230° and 320-410° for $\varphi_{0^\circ, 180^\circ}$, respectively. As shown in Figure 10 (B), the $f_{90^\circ, 270^\circ}$ and $f_{0^\circ, 180^\circ}$ values are in the range 0.03-0.22 and -0.04 to -0.06, respectively, which are quite small as compared to those of the perfectly parallel- and perpendicular-oriented lamellae. This indicates that the remaining stress can induce only small amount of lamellar microdomains performing the preferential orientation with mostly in the parallel directions to the SD. It should be noted that the $f_{90^\circ, 270^\circ}$ values are increased with an increase of the take-up velocity, and remained almost constant at the take-up velocity above 620 m/min. However, $f_{0^\circ, 180^\circ}$ values only slightly dropped at the take-up velocity above 620

m/min. This indicates that the applied stress is store in the SEBS chain, and, after thermal treatment, it causes the chain relaxation leading to rearrangement of microdomains, from short- to long-range ordered ones, with traces of preferential orientations.

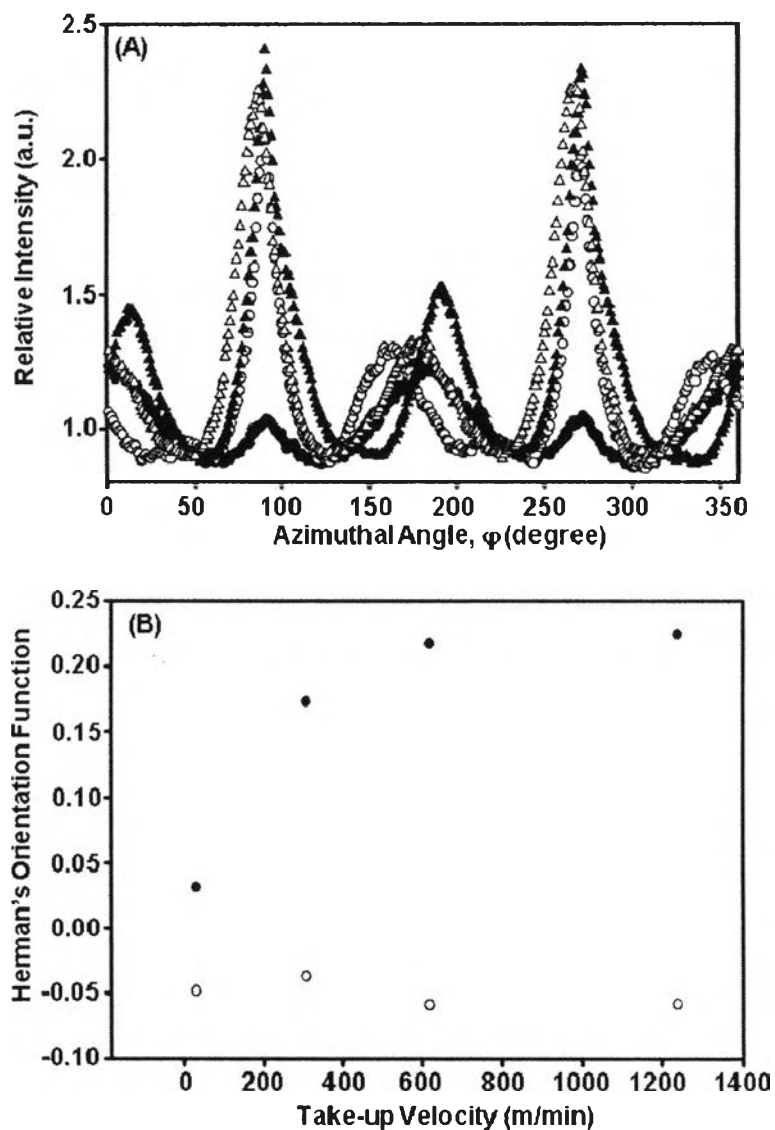


Figure 4.10 Relative intensity distribution as a function of the azimuthal angle φ along the first-order peak (azimuthal scan) (a) in the 2D-SAXS pattern of post-cured S75BZ25 electrospinning fibers collected at: (●) 31.5 m/min, (○) 310 m/min, (▲) 620 m/min and (Δ) 1240 m/min, and Herman's orientation functions (f) for the peaks of the azimuthal scan at $\varphi = 90^\circ$ (●) and at $\varphi = 0^\circ$ (○) of post-cured S75BZ25 electrospinning fibers collected at various take-up velocities.

4.5 Conclusions

Bisphenol-A based benzoxazines showed a strong interaction with SEBS via π - π interaction. This brought physical-crosslink networks to PS segments in SEBS chains resulting in vitrified PS microdomains. The microdomain orientation of SEBS was responsive to the stress initiated by rotational-disk collector. The velocity of collector, i.e. take-up velocity, is another key factor to direct the microdomain orientation of SEBS as evidenced from an optimal velocity (310 m/min) leading to a microdomain orientation with a parallel direction to the fiber axis. The velocity above this level was found to initiate the rupture of the physical crosslink network as seen from the change from parallel align to randomly aligned lamellar microdomain orientation. Thermal treatment of SEBS containing BZ not only initiated the curing of BZ to be polyBZ but also annealing SEBS. After thermal treatment, for fibers, their microdomain became random but some traces of orientation in parallel and perpendicular to the fiber axis remained. For polyBZ, the nanospheres (~80nm) thermosetting resins were obtained and this will be reported in our up-coming article. The present work shows a model case to control the microdomain orientation for the electrospun fibers. The SEBS electrospun fiber containing BZ under macroscopic external stimulus of stretching force along with a specific interaction at molecular level of π - π interaction between SEBS and BZ proved to us that we could direct the microdomain orientation to be almost perfectly parallel to the fiber axis.

4.6 Acknowledgements

S. C. and W. R. would like to express theirgratefulto the Thailand Research Fund (the Royal Golden Jubilee Ph.D Scholarship, grant no. PHD/0058/2550), and the Japan Student Services Organization (JASSO) for the financial.The SEBS was kindly supplied by Asahi Kasei Chemicals Corporation, Japan. The SAXS experiments were conducted at the SPring-8 with the approved number

2009A1153. Furthermore, S. C. and W. R would like to thank Takuma Shimojima and Go Kimura for SAXS measurement and data process.

4.7 References

1. Holden, G.; Kricheldorf, H. R.; Quirk, R. P. In *Thermoplastic Elastomers*, Edition 3rd, Hanser Verlag **2004**; p 2-3.
2. Bhowmick, A. K.; Stephens, H. L. In *Handbook of Elastomers*, Edition 2nd, CRC Press **2000**; p 327-330.
3. J A Brydson, Rapra Technology Limited, In *Thermoplastic Elastomers: Properties and Applications*, iSmithers Rapra Publishing **1995**; 3-7.
4. Wang, Y.; Hong, X.; Liu, B.; Ma, C.; Zgang, C. *Macromolecules* **2008**, 41, 5799-5808.
5. Heck, B.; Arends, P.; Ganter, M.; Kressler, J.; StÜhn, B. *Macromolecules* **1997**, 30, 4559-4566.
6. Figueiredo, P.; Geppert, S.; Brandsch, R.; Bar, G.; Thomann, R.; Spontak, R.J.; Gronski, W. *Macromolecules* **2001**, 34, 71-180.
7. Shefelbine, T. A.; Vigild, M. E.; Hajduk, D. A.; Hillmyer, M. A.; Cussler, E. L.; Bate, F. S. *J. Am. Chem. Soc.* **1999**, 121 (37), 8457-8465.
8. Ma, M.; Titievsky, K.; Thomus, E. L.; Rutledge, G. C. *Nano Letter* **2009**, 9, 4, 1678-1683.
9. Honeker, C. C.; Thomas, E. L. *Chem. Mater* **1996**, 8, 1702-1714.
10. Kalra, V.; Kakad, P. A.; Mendez, S.; Ivannikov, T.; Kamperman, M.; Joo, Y. *L. Macromolecules* **2006**, 39, 5453-5457.

11. Sakurai, S.; Momii, T.; Taie, K.; Shibayama, M.; Nomura, S. *Macromolecules* **1993**, *26*, 485-491.
12. Sakurai, S.; Aida, S.; Okamoto, S.; Ono, T.; Imaizumi, K.; Nomura, S. *Macromolecules* **2001**, *34*, 3672-3678.
13. Wang, J. Y.; Chen, W.; Russell, T. P. *Macromolecules* **2008**, *41* (19), 7227-7231.
14. Ramakrishna, S.; Fujihara, K.; Teo, W.E.; Teo, T.E.; Ma, Z. In *An Introduction to Electrospinning and Nanofibers*, World Scientific Publishing Co. Pte.Ltd. **2005**.
15. Fong, H.; Reneker D. H. *J. Polymer Sci. B Polymer Phys* **1999**, *37*, 3488-3493.
16. Ma, M.; Hill, R. M.; Lowery, J. L.; Fridrikh, S. V.; Rutledge, G. *C.Langmuir*. **2005**, *21*, 5549.
17. Ma, M.; Krikorian, V.; Yu, J. H.; Thomas, E. L.; Rutledge, G. *C.Nano Letters* **2006**, *6*, 12, 2969-2972.
18. Rungswang, W.; Kotaki, M.; Sakurai, S.; Shimojima, T.; Kimura, G.; Chirachanchai, S. Accepted by *Polymer*.
19. Ning, X.; Ishida, H. *J. Polymer Sci. B Polymer Phys*, **1994**, *32*, 921-927.
20. Ishida, H. US Patent 5, 543, 516, 1996.
21. Ishida, H.; Sanders, D. P. *Macromolecules* **2000**, *33*, 8149-8157.
22. Takeichi, T.; Agag, T. *High Performance Polymer* **2006**, *18*, 777-797.
23. Chaisuwan, T.; Ishida, H. *J. App. Pol. Sci.* **2006**, *101*, 548-558.
24. Agag, T.; Takeichi, T. *Macromolecules* **2003**, *36*, 6010-6017.

25. Rungswang, W.; Chirachanchai, S. *Macromol. Mater. Eng.* **2010**, 295, In Press.
26. Foster, R. *Chem. Br.* **1976**, 12, 18.
27. Reczek, J. J.; Iverson, B. L. *Macromolecules* **2006**, 39, 5601-5603.
28. Fisk, C. L.; Becker, E. D.; Miles, H. T.; Pinnavaia, T. J. *J. Am. Chem. Soc.* **1982**, 104, 3307-3314.
29. Mo, H.; Pochapsky, T.C. *Progress in Nuclear Magnetic Resonance Spectroscopy* **1997**, 30, 1-38.
30. Hiki, Y.; Kosugi, T. *J. Non-Cryst. Solids*. **2005**, 351, 1300-1306.
31. Hiki, Y.; Kogure, Y. *J. Non-Cryst. Solids*. **2003**, 315, 63-69.
32. Sakurai, S.; Sakamoto, J.; Shibayama, M.; Nomura, S. *Macromolecules* **1993**, 26, 3351-3356.
33. Sakurai, S.; Aida, S.; Okamoto, S.; Sakurai, K.; Nomura, S. *Macromolecules* **2003**, 36, 1930-1939.